NJC

Accepted Manuscript

This article can be cited before page numbers have been issued, to do this please use: J. Han, Y. Cai, Y. Wang, X. Dai, L. Wang, C. Li, B. An and L. Ni, *New J. Chem.*, 2018, DOI: 10.1039/C8NJ01917G.

ROYAL SOCIETY OF CHEMISTRY

rsc.li/njc

View Article Online
DOI: 10.1039/C8NJ01917G

Mixed polymeric micelles as multifunctional visual thermo-sensor for rapid analysis of mixed metal ions with Al^{3+} and Fe^{3+}

Juan Han[a], Yunfeng Cai[a], Yun Wang[b,*], Xiaohui Dai[b], Lei Wang[b], Chunmei Li[b], Baodong An[b], Liang Ni[b]

[a] *School of Food and Biological Engineering, Jiangsu University, Zhenjiang 212013, PR China*

[b] *School of Chemistry and Chemical Engineering, Jiangsu University, Zhenjiang 212013, PR China*

**Corresponding authors.* Yun Wang, Tel.: +86-0511-88790683, *E-mail addresses:* yunwang@ujs.edu.cn.

Abstract:

A novel type of responsive mixed double hydrophilic block copolymers (DHBC)-based multifunctional visual thermo-sensor (the mixed copolymers of poly(ethylene oxide)-b-poly(N-isopropylacrylamide-co-2,4-methacryloyl benzaldehyde oxime) (PEG-b-P(NIPAM-co-BDMa) and poly(ethylene oxide)-b-poly(N-isopropylacrylamide-co-rhodamine 6G methyl acrylic acid) (PEG-b- P(NIPAM-co-Rh6GEMa) for the detection of Al^{3+} and Fe^{3+} was designed and synthesized based on the reversible addition-fragmentation chain transfer (RAFT) polymerization. The studies of sensing processes showed that the multifunctional visual thermo-sensor had excellent selectivity for Al^{3+} and Fe^{3+} ions over many environ-mentally relevant ions, and high

View Article Online
DOI: 10.1039/C8NJ01917G

sensitivity with the detection limit in nanomolar level. Moreover, the multifunctional visual thermo-sensor can form the micelles with (P(NIPAM-co-BDMa)/P(NIPAM-co-Rh6GEMa) blocks as cores and well-solvated PEG block as coronas when increasing the temperature, which can enhance the detection sensitivity of Al^{3+} and Fe^{3+} ions. The detection limit of 0.05 g/L mixed micelles for the analysis of Al^{3+} and Fe^{3+} ions from 25 °C to 40 °C were decreased from ~5.95 to ~4.02 nM, ~30.30 nM to ~23.84 nM, respectively. Furthermore, mixed micelles combined with Principal Component Analysis (PCA) and linear regression analysis to establish prediction models to achieve quantitative detection of the mixed ions with Al^{3+} and Fe^{3+} successfully.

Key words:

multifunctional visual thermo-sensor, Al^{3+}, Fe^{3+}, PCA

Introduction

Fluorescence chemosensors as valuable tools which have some excellent properties, such as high selectivity, high sensitivity, fast response, low cost and easy operation, have been widely researched and applied in many environmental and biological processes[1-4]. Recently, more and more researchers focus on the design of dual or multi metal ion fluorescence chemosensor comparison with the single response probes appears to be a new area of research. The dual or multi fluorescence chemosensor have the wider potential applications in analyte recognition due to it provides an edge over the single response probes in terms of cost-effectiveness and efficient analysis in fields.

Aluminum and Iron element play the very important roles in biological and environmental systems[5-8]. Aluminum is the largest metal element in nature and is extensively used in our daily life, such as aluminum-based pharmaceuticals and storage/cooking utensils which results in a moderate increase in the Al^{3+} concentration in food. Due to the large number of the use of aluminum foil and aluminum containers, the possibility of the body to absorb the Al^{3+} increase a lot correspondingly[5]. Conversely, Iron is not only one of the most common transition metal, is essential for

View Article Online
DOI: 10.1039/C8NJ01917G

all living organisms, but also the highest content of trace elements in the body, and it is involved in the composition of the body of a variety of key enzymes and proteins [9, 10]. However, excessive intake of Al^{3+} and Fe^{3+} may lead to a wide range of numerous diseases such as heart disease, Alzheimer's disease, osteoporosis, Parkinson's disease and malfunctions of the central nervous system[11-14]. Thus, it is urgent to develop high selectivity and sensitivity chemosensors for the effective detection of Al^{3+} and Fe^{3+} in the environment and biological samples.

As we all know, Al^{3+} has reverse magnetic properties, and the probe is mostly fluorescent enhanced probe[15-17]. Fe^{3+} has paramagnetic characteristics, which usually makes many fluorescent probes with Fe^{3+} show fluorescence quenching, which seriously affects the sensitivity of detection[18-20]. Thus, the fluorescent molecular probe based on a single emission mechanism for detecting Al^{3+} and Fe^{3+} is relatively few. He et al. reported that a novel bis-rhodamine urea BRU could efficiently recognize Fe^{3+} and Al^{3+} in CH_3OH/H_2O through a turn-on colorimetric response [21]. Kang et al. synthesized a MOF-based sensor which could recognize Fe^{3+} by the quenching of Eu^{3+} emission and detect Al^{3+} by the enhancement of the ligand-based emission [22]. And a perylenediimide (PDI)-based host receptor which exhibits excellent sensitivity towards Al^{3+} and Fe^{3+} in DMSO was reported by Suganya et al [23]. However, these small molecule-based fluorescence chemosensors for detection of Al^{3+} and Fe^{3+} ions have some limitations, including poor water solubility and biocompatibility, unsatisfied detection sensitivity, and difficult to achieve the multifunctional integration with other analyte-sensing capabilities. And what's more, although these probes can detect Fe^{3+} and Al^{3+}, there are no probes that can simultaneously determine the contents of these two coexisting metals without interfering with each other.

In the past two decades, in order to achieve functional cooperativity and broader adaptability of probe, the topic of self-assembled has become increasingly hot, and gradually tends to the study of stimuli-responsive double hydrophilic block copolymers (DHBCs)[24-27]. It can automatically self-assemble into one or more types of aggregates in aqueous solution when suffering proper external stimuli such as pH,

View Article Online
DOI: 10.1039/C8NJ01917G

temperature and ionic strength. Thus, we integrate sensitive primers into amphiphilic polymers to develop multiple functional (temperature, ions, etc.) probes to offer a series of potential features such as improved water solubility, enhanced detection sensitivity, excellent biocompatibility.

Visual detection has received widespread attention because of the extreme simplicity and low cost of this type of assay in which the presence of target analyte can be directly observed by the naked eye based on color changes[28, 29]. Because both qualitative and semiquantitative assessment can be performed in real time without using any complex and expensive instrument, visual detection is especially important in field analysis of point-of-care test and environmental monitoring. Based on this, we proposed to combine the multifunctional macromolecule fluorescence probe with the visual detection to obtain the multifunctional visual thermo-sensor. By designing the detection model rationally and extracting the eigenvalues of the color, the Principal Component Analysis (PCA) analysis method is constructed to realize the simultaneous quantitative detection Al^{3+} and Fe^{3+}.

Herein, we report on the utilization of mixed micelles as a multifunctional visual thermo-sensor for the efficiently detection of Al^{3+} and Fe^{3+} (Scheme 1). Two novel types of responsive DHBCs-based chemosensors, poly(ethylene oxide)-b-poly(N-isopropylacrylamide-co-2,4-Methacryloyl Benzaldehyde Oxime)$_{60}$ (PEG_{113}-b-P(NIPAM-co-BDMa)$_{60}$), poly(ethylene oxide)-b-poly(N-isopropylacrylamide-co-Rhodamine 6G Methyl Acrylic Acid)$_{67}$ (PEG_{113}-b-P(NIPAM-co-Rh6GEMa)$_{67}$) were designed and synthetized by reversible addition-fragmentation chain transfer (RAFT) polymerization, and Al^{3+} and Fe^{3+} recognition primitives BDMa and Rh6GEMa were labeled in the thermosensitive block, respectively. The sensing capabilities and the effects of reaction time and system temperature of the sensor were discussed. In addition, based on the identification of different colors of Al^{3+} and Fe^{3+} (mixed micelles for Al^{3+} and Fe^{3+} were made of blue and yellow fluorescence, respectively), quantitative prediction models were constructed for simultaneous analysis to detect the respective contents of

View Article Online
DOI: 10.1039/C8NJ01917G

the two metal ions in the mixture.

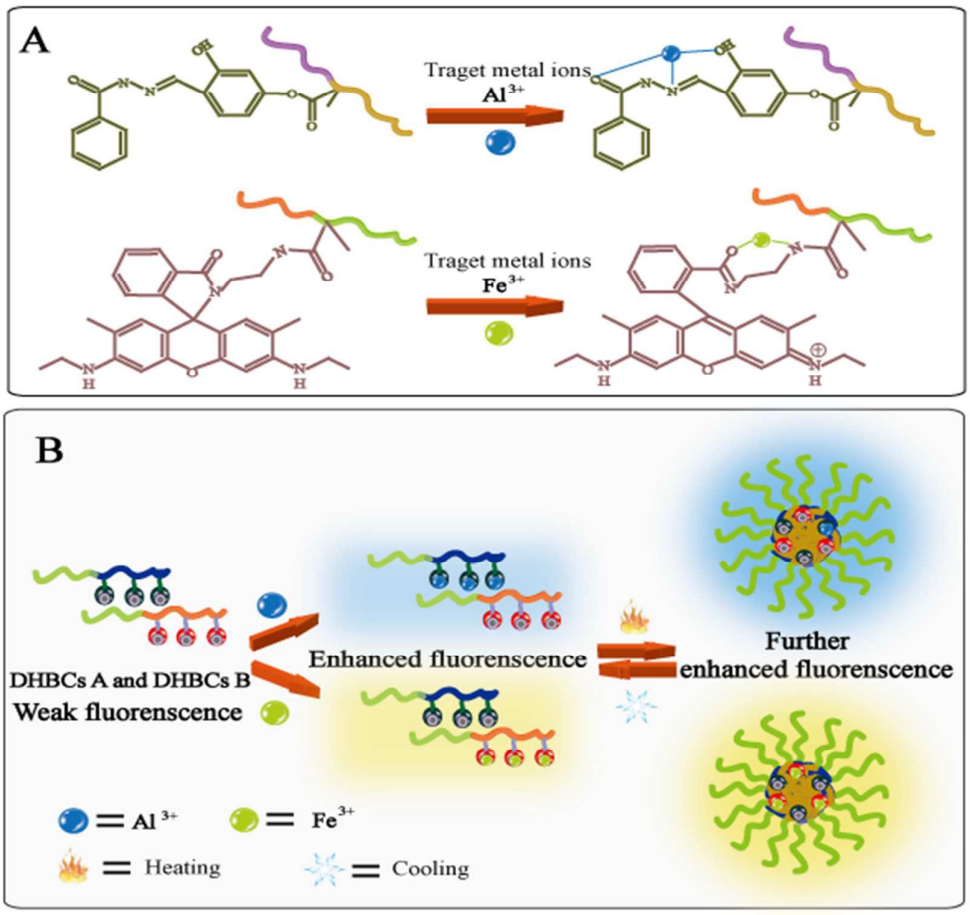

Scheme 1. (A) Schematic illustration for the metal ion response mechanism, (B) Schematic illustration for the fabrication of thermos-responsive PEG_{113} -b-P(NIPAM-co-BDMa)$_{60}$ and PEG_{113} -b-P(NIPAM-co-R6GEMa)$_{67}$ mixed sensors.

2. Experimental

2.1 Materials

Poly(ethylene oxide) monomethyl ether (PEO_{113}-OH, *M*n = 5.0 kDa, *M*w/*M*n = 1.05; mean degree of polymerization, DP, is 113) purchased from Aldrich was used as received (www. sigmaaldrich.com). N-Isopropylacrylamide (NIPAM, 97 %) purchased from Aldrich was recrystallized twice by a mixture of n-hexane and benzene (v/v=2:1) prior usage. 4-(dimethylamino) pyridine (DMAP, ≥ 99 %), Benzohydrazide (≥ 99 %), dicyclohexylcarbodiimide (DCC, ≥ 99 %), 2,4-dihydroxyformaldehyde (≥ 98 %), 3-mercaptopropionic acid (MPA, ≥98%),

View Article Online
DOI: 10.1039/C8NJ01917G

Rhodamine 6G (≥ 99 %), Ethylenediamine (≥ 98 %), methacryloyl chloride (≥ 95 %), Azoisobutyronitrile (AIBN, ≥ 98 %) and all other reagents purchased from Sinopharm Chemical Reagent Co. were used as received (www.en.reagent.com.cn). Methacryloyl chloride was distilled prior usage. AIBN was recrystallized from 95% ethanol. Dichloromethane (CH_2Cl_2) were dried over CaH_2 and distilled just prior usage. Toluene was distilled over sodium and benzophenone immediately before usage. Salts (K^+, Na^+, Li^+, Co^{2+}, Sr^{2+}, Ba^{2+}, Ca^{2+}, Cd^{2+}, Ni^{2+}, Mn^{2+}, Fe^{2+}, Cu^{2+}, Fe^{3+}, Cr^{3+}, Zn^{2+}, Al^{3+}) were used for experiments. Water was deionized with a Milli-Q SP reagent water system (Millipore, Bedford, MA, USA, www.millipore.bioon.com.cn) to a specific resistivity of 18.4 MΩ cm.

2.2 Sample synthesis

In order to prepare mixed micelles with multiple reactions of metal ions and temperature, the target PEG_{113}-b-P(NIPAM-co-BDMA)$_{60}$ and PEG_{113}-b-P(NIPAM-co-Rh6GEMa)$_{67}$ were obtained.

2.2.1 Synthesis of BDMa (Scheme 2(a) and (b))

Benzohydrazide (1.36 g, 0.01 mol) was dissolved in ethanol (20.00 mL), and a mixed solution of 2,4-dihydroxybenzaldehyde (1.38 g, 0.01 mol) and ethanol (20.00 mL) was added dropwise with stirring. Then the temperature was raised to 60 °C and stirred for 1 hour. The solid was precipitated and filtered to obtain a crude product which was recrystallized three times in ethanol to give scaly rose gold solid product 2,4-dihydroxybenzaldehyde oxime (BD) (2.04 g, yield: 80.0 %). ^{1}H NMR (CD_3OD, δ, ppm; Fig. S1 (a)): 8.41 (1H, ArCH=N-), 7.90-7.95 (2H, ArH), 7.50-7.65 (3H, ArH), 7.22 (1H, ArH), 6.35-6.45 (2H, ArH).

The product BD (2.00 g, 7.84 mmol) and triethylamine (0.79 g, 7.84 mmol) were dissolved in CH_2Cl_2 (30.00 mL), followed by the dropwise addition of salicylaldehyde (0.81 g, 7.84 mmol) in the ice bath. The reaction was refluxed at 25.0 °C for 3 h. The reaction mixture was washed with Na_2HCO_3 aqueous solution for three times. The organic layer was dried over anhydrous sodium sulfate and filtered, and the filtrate was subjected to rotary evaporation to give the crude product which

View Article Online
DOI: 10.1039/C8NJ01917G

was finally dissolved in an appropriate amount of CH_2Cl_2. The product was precipitated by adding excess ethanol and filtered again, the reaction was repeated three times to obtain yellowish solid powder BDMa (1.01 g, yield: 40.0 %). ^{1}H NMR (CD_3OD, δ, ppm; Fig. S1(b)): 8.51 (1H, ArCH=N-), 8.32 (1H, ArH), 7.93 (2H, ArH), 7.62 (1H, ArH), 7.52 (1H, ArH), 7.18 (1H, ArH), 7.10 (1H, ArH), 5.37 (1H, -C(CH_3)=CHH), 5.88 (1H, -C(CH_3)=CHH), 2.07 (3H, CH_3C-).

2.2.2 Synthesis of Rh6GEMa (Scheme 2(c) and (d))

Rhodamine 6G (4.80 g, 10.00 mmol) was dissolved in absolute ethanol (60.00 mL), followed by the dropwise addition of ethylenediamine (5.00 mL) under stirring. The reaction was refluxed at 70.0 ℃ for 12 h. The solid obtained by removing the solvent by rotary evaporation was recrystallized three times in ethanol. Finally, the resulting powder was dried in a vacuum oven to obtain dried solid Rhodamine 6G hydrazide (Rh6GEda) (3.43 g, yield: 75.0 %). ^{1}H NMR (DMSO-d_6, δ, ppm, TMS; Fig. S1(c)): 7.94 (1H, ArH), 7.47 (2H, ArH), 7.07 (1H, ArH), 6.36 (2H, ArH), 6.24 (2H, ArH), 3.53 (2H, -CH_2-), 3.15-3.25 (4H, -CH_2-), 2.36 (2H, -CH_2-), 1.91 (6H, -CH_3), 1.34 (6H, -CH_3).

Rh6GEda (0.28 g, 5.00 mmol) and triethylamine (0.63 g, 6.00 mmol) were dissolved in CH_2Cl_2 (80 mL), followed by the dropwise addition of the mixture of methacryloyl chloride (0.52 g, 5.00 mmol) and CH_2Cl_2 (30 mL) in the ice bath within 1 h. The new mixture was reacted at 25.0 ℃ for 3 h. Then the reaction mixture was washed with Na_2HCO_3 aqueous solution for three times. The organic layer was dried over anhydrous sodium sulfate and filtered, and the filtrate was subjected to rotary evaporation to give the crude product which was recrystallized from acetonitrile and dried in vacuo to give pale pink solid Rh6GEMa (1.83 g, 69.8 %). ^{1}H NMR ($CDCl_3$, δ, ppm, TMS; Fig. S1(d)): 8.02 (1H, ArH), 7.58 (2H, ArH), 7.32 (1H, ArH), 6.85-7.15 (3H, ArH), 6.50 (1H, ArH), 5.78 (1H, -C(CH_3)=CHH), 5.35 (1H, -C(CH_3)=CHH), 2.75-4.00 (8H, -CH_2-), 2.01 (9H, -CH_3), 1.21 (6H, -CH_3)

2.2.3 Synthesis of Carboxyl-containing trithiocarbonates (BTPA) (Scheme 2(e))

BTPA was prepared by adding MPA (2.50 mL, 28.65 mmol) into aqueous KOH

View Article Online
DOI: 10.1039/C8NJ01917G

(1.84 mol/L, 31.25 mL) aqueous solution, then dropped CS_2 (3.65mL). After stirring for 5 h, dropped benzyl bromide (4.95 g, 28.65 mmol), heating up to 80.0 °C for 12 h. After reaction, on cooling to room temperature, an excess amount of hydrochloric acid acidification was added into the reaction solution. With the addition of chloroform (90.00 mL), separate organic phase washing with 10 % Na_2CO_3 aqueous solution. Remove organic solvents. The yellow solid was recrystallized by CH_2Cl_2 for three times. Finally product of 3.20 g was obtained and yield was about 40.9 %. ^{1}H NMR ($CDCl_3$, δ, ppm, TMS; Fig. S1 (e)): 7.33 (5H, ArH), 4.64 (2H, $ArCH_2$-), 3.65 (2H, -C(=S)SCH_2-), 2.88 (2H, -C(=S)SCH_2CH_2CO-).

2.2.4 Synthesis of PEO-based MacroRAFT agent (Scheme 2(f))

PEO-based macroRAFT agent was prepared the esterification reaction between PEO_{113}-OH and BTPA in the presence of water removal agent DCC and catalyzer DMAP. After PEO_{113}-OH (5.00 g, 1.00 mmol) dissolved in anhydrous toluene (25.00 mL), the mixture was settled by azeotropic distillation at 50.0 °C under reduced pressure (relative vacuum degree: -0.09851 MPa) to remove most of the solvent. Then dry BTPA (0.55 g, 2.00 mmol) and CH_2Cl_2 (50.00 mL) were added and the mixture was placed in an ice-water bath keeping 0.0 °C. Then another mixture of DCC (0.42 g, 2.00 mmol), DMAP (25 mg, 0.20 mmol) dissolved in dry CH_2Cl_2 (10.00 mL) was added dropwise over 1 h. The reaction mixture was stirred at room temperature for 48 h. Insoluble salts were removed by filtration and the filtrates were concentrated on a rotary evaporator and then precipitated into an excess of cold diethyl ether obtaining powder at last. The powder settled with the dissolution-precipitation cycle mentioned above for three times. After drying in a vacuum oven overnight at room temperature, PEO_{113}-based macroRAFT agent was obtained as a slightly yellowish powder (4.80 g, yield: 62%). Gel Permeation Chromatography (GPC) analysis revealed an *M*n of 6.1 kDa and an *M*w/*M*n of 1.06 (Fig. S2 (a)). ^{1}H NMR ($CDCl_3$, δ, ppm, TMS; Fig. S1 (f)): 7.33 (5H, ArH), 4.60 (2H, $ArCH_2$-), 4.27 (2H, -CH_2OCOCH_2-), 3.83-3.58 (2H, -CH_2CH_2O-), 3.54 (3H, CH_3O-), 3.38 (2H, -$CH_2OCOCH_2CH_2SC$(=S)-), 2.82 (2H, -$CH_2OCOCH_2CH_2SC$-(=S)-).

View Article Online
DOI: 10.1039/C8NJ01917G

2.2.5 Synthesis of PEG_{113}-b-P(NIPAM-co-BDMa)$_{60}$ (Scheme 2(g))

The RAFT synthesis of BDMa-labeled DHBCs, PEG_{113}-b-P(NIPAM-co-BDMa)$_{60}$ was as follows: dry NIPAM (0.91 g, 8.00 mmol), BDMa (0.10g, 0.32 mmol), PEO-based macroRAFT agent (0.42 g, 0.08 mmol), AIBN (2.00 mg, 12.00 μmol), and 1,4-dioxane (1.40 g) were added in a reaction tube equipped with a magnetic stirring bar. The tube was carefully degassed by three freeze-pump-thaw cycles and then sealed under vacuum. Stirring for 1.5 h at 70 °C in an oil bath, the reaction tube was quenched into liquid nitrogen. Then the reaction mixture was diluted with proper 1,4-dioxane and then precipitated into an excess of cool diethyl ether. The above dissolution-precipitation cycle was repeated for three times. PEG_{113}-b-P(NIPAM-co-BDMa)$_{60}$ was obtained as yellowish powder with a yield of 63% (0.84 g). GPC analysis revealed an *M*n of 13.2 kDa and an *M*w/*M*n of 1.14 (Fig. S2 (b)). The degree of polymerization, DP, of P(NIPAM-co-BDMa) was determined to be 60 by ^{1}H NMR analysis (Fig. S1 (g)). Thus, the polymer was denoted as PEG_{113} -b-P(NIPAM-co-BDMa)$_{60}$. BDMa content in 0.05g/L P(NIPAM-co-BDMa) block was determined to be 5.02μmol/L by a spectrofluorometer by using BDMa as the calibration standard in the presence of 4 equiv (1.0 equiv relative to the BDMa moiety) of Al^{3+} ions.

2.2.6 Synthesis of PEG_{113}-b-P(NIPAM-co-Rh6GEMa)$_{67}$ (Scheme 2(h))

The RAFT synthesis of Rh6GEMa-labeled DHBCs, PEG_{113}-b-P(NIPAM-co-Rh6GEMa)$_{67}$ was as follows: dry NIPAM (0.91 g, 8.00 mmol), Rh6GEMa (0.19 g, 0.32 mmol), PEO-based macroRAFT agent (0.42 g, 0.08 mmol), AIBN (2.00 mg, 12.00 μmol), and 1,4-dioxane (1.40 g) were added into a reaction tube equipped with a magnetic stirring bar. The tube was carefully degassed by three freeze-pump-thaw cycles and then sealed under vacuum. Stirring for 1.5 h at 70 °C in an oil bath, the reaction tube was quenched into liquid nitrogen. Then the reaction mixture was diluted with proper 1,4-dioxane and then precipitated into an excess of cool diethyl ether. The above dissolution-precipitation cycle was repeated for three times. PEG_{113}-b-P(NIPAM-co-Rh6GEMa)$_{67}$ was obtained as yellowish

View Article Online
DOI: 10.1039/C8NJ01917G

powder with a yield of 63 % (0.84 g). GPC analysis revealed an *M*n of 13.1 kDa and an *M*w/*M*n of 1.15 (Fig. S2 (c)). The degree of polymerization, DP, of P(NIPAM-co-BDMa) was determined to be 67 by ^{1}H NMR analysis (Fig. S1 (h)). Thus, the polymer was denoted as PEG_{113} -b-P(NIPAM-co-Rh6GEMa)$_{67}$. Rh6GEMa content in 0.05 g/L P(NIPAM-co-Rh6GEMa) block was determined to be 14.98 μmol/L by a spectrofluorometer by using Rh6GEMa as the calibration standard in the presence of 6 equiv (1.0 equiv relative to the Rh6GEMa moiety) of Fe^{3+} ions.

2.2.7 Configuration of fluorescent sensor array and processing of data

0.05 g/L multifunctional visual thermo-sensor was mixed by PEG_{113}-b-P(NIPAM-co-BDMa)$_{60}$ and PEG_{113}-b-P (NIPAM-co-R6GEMa)$_{67}$ at 25 ℃ with a buffer solution (10 mM HEPES, pH 7.4). First of all, take a 0.8 mL of the solution as blank control. In addition, another 24 samples were placed in a 96-well Perspex plate according to the Table 1 and added a certain amount of Al^{3+} and Fe^{3+} to the final concentration as shown in the Table 1. These samples are used as templates for full fluorescent color development and to constitute a visual sensor.

Table 1 The arrangement of mixed metal ions with Al^{3+} and Fe^{3+}

		Concentration of Al^{3+} (μM)					
		5	**10**	**15**	**20**	**25**	**30**
Concentration of Fe^{3+}(μM)	**5**	1	2	3	4	5	6
	10	7	8	9	10	11	12
	15	13	14	15	16	17	18
	20	19	20	21	22	23	24

Data acquistion and processing are carried out by the smartphone/fluorescent sensor array ensemble designed by our research group. The 96-well Perspex tablet is transferred to the box, and the smartphone is always fixed at the top. With this equipment, ambient lighting condition and imaging distance/angle were kept constant when capturing the images of the sensor arrangement. The “before” image consisted

View Article Online
DOI: 10.1039/C8NJ01917G

of a shot taken with the 13 mega pixel (MP) smartphone camera capturing the color of the individual mixed micelles aqueous solution; the "after" image consisted of a camera shot directed towards the combination of the mixed micelles and hybrid ions. Using our laboratory designed app on the smartphone, a color difference map was obtained by subtracting the "before" image from the "after" image (red minus red, green minus green, blue minus blue). To prevent subtraction artifacts caused by acquisitions near the spot edge, only the spot center was included in the calculation. All experiments were run in quintuplicate for each of the 24 analytes and the blank control. Next, the ΔRGB (Red, Green, Blue) data were processed by PCA and linear regression analysis.

Likewise, the images and data of the 12 analytes in the validation test were also obtained.

View Article Online
DOI: 10.1039/C8NJ01917G

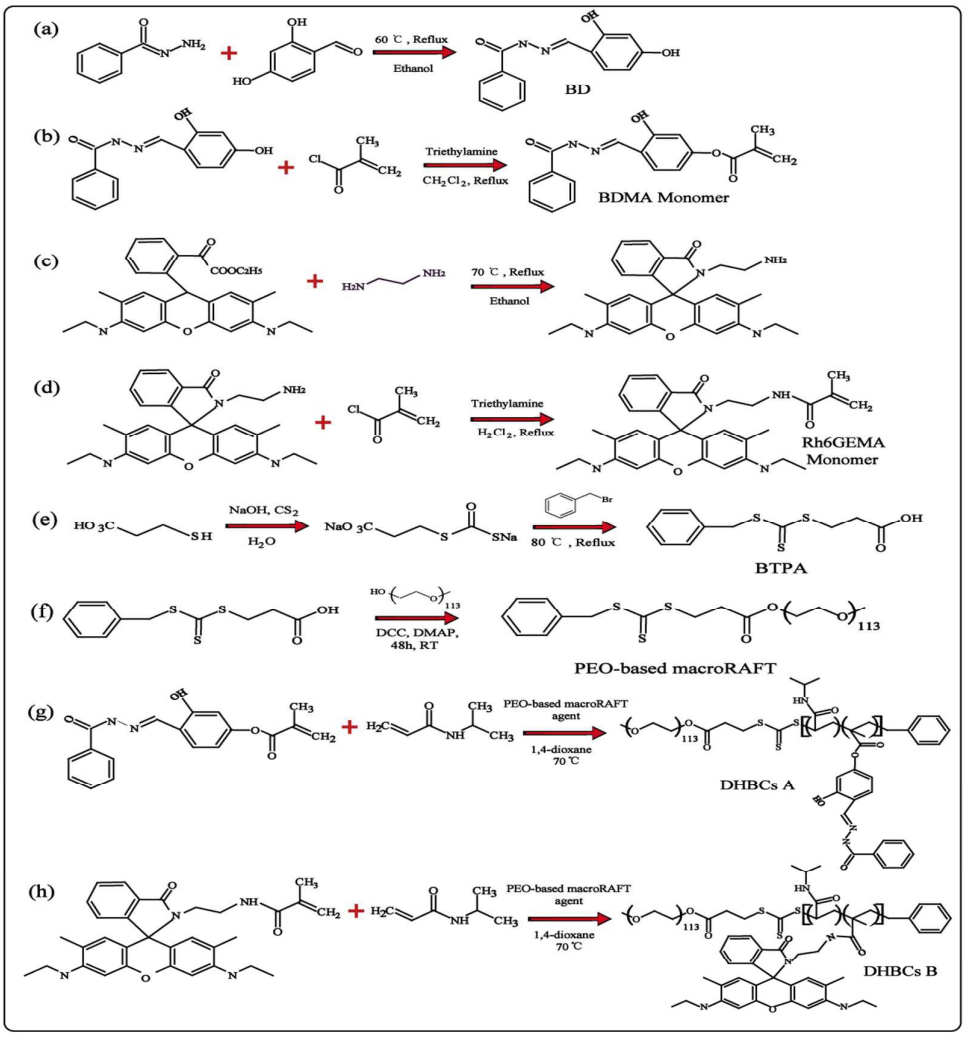

Scheme 2. Schematic illustration for the synthesis of the thermoresponsive PEG_{113} -b-P(NIPAM-co-BDMa)$_{60}$ and PEG_{113} -b-P(NIPAM-co-R6GEMa)$_{67}$.

2.3 Characterization

Nuclear Magnetic Resonance (H NMR) Spectroscopy. All ^{1}H NMR spectra were recorded on a German BRUKERAC-P400 type nuclear magnetic resonance (resonance frequency of 400 MHz for ^{1}H) operated in the Fourier transform mode. $CDCl_3$, CD_3OD and DMSO-d_6 were used as the solvents.

Gel Permeation Chromatography (GPC). Molecular weights and molecular weight distributions were determined by gel permeation chromatography (GPC) equipped with a LC20 high performance liquid chromatography pump and a RID-20 differential refractive index detector (Japan Shimadzu Company). It used an American HR4 Styragel columns at an oven temperature of 35 °C. The eluent was THF at a flow

View Article Online
DOI: 10.1039/C8NJ01917G

rate of 1.0 mL/min. A series of low-polydispersity poly-styrene standards were employed for calibration.

Laser Light Scattering (LLS). Dynamic and static LLS measurements were conducted on a commercial spectrometer (ALV/DLS/SLS-5022F) equipped with a multitau digital time correlator (ALV5000) and a cylindrical 22 mW UNIPHASE He-Ne laser (λ_0 = 632 nm) as the light source.

Fluorescence Measurements. Fluorescence signals were measured on a Cary Eclipse luminescence spectrometer (Varian, USA) equipped with a xenon flash lamp and a computer. The temperature of the water-jacketed cell holder was controlled by a programmable circulation bath. The slit widths were set at 5 nm for excitation and 2.5 or 5 nm for emission.

Use Huawei Imagination 6S as a camera, image analysis using self-developed mobile phone image processing software.

3. Results and discussion

The structures of two thermosensitive double hydrophilic block copolymers (PEG_{113}-b-P(NIPAM-co-BDMa)$_{60}$ and PEG_{113}-b-P(NIPAM-co-Rh6GEMa)$_{67}$) which were synthesized by RAFT were characterized by ^{1}H NMR and GPC. The structural parameters of these two copolymers were shown in Table 2. The content of BDMa and Rh6GEMa in (PEG_{113}-b-P(NIPAM-co-BDMa)$_{60}$ and PEG_{113}-b-P(NIPAM-co-Rh6GEMa)$_{67}$ were calculated to be ~2.21 mol% and ~5.86 mol%, respectively. There results were in good agreement with their structures showed in Scheme 2.

Table 2 Summary of structural parameters of diblock copolymers synthesized in this work

Samples	DP_{NMR}[a]		M_n[b] (kDa)	PDI[b]
	PEG block	PNIPAM block		
PEG_{113}-based MacroRAFT agent	113	/	6.1	1.06
PEG_{113}-b-P(NIPAM-co-BDMa)$_{60}$	113	60	13.2	1.14
PEG_{113}-b-P(NIPAM-co-Rh6GEMa)$_{67}$	113	67	13.1	1.15

[a] Determined by ^{1}H NMR characterization in $CDCl_3$. [b] Obtained from GPC analysis using as

View Article Online
DOI: 10.1039/C8NJ01917G

eluent at a flow rate of 1.0 mL/min.

3.1 Fluorescence spectral characteristics

The photo-physical complexation studies of multifunctional visual thermo-sensor with a series of different metal such as K^+, Na^+, Li^+, Ca^{2+}, Sr^{2+}, Ba^{2+}, Co^{2+}, Fe^{2+}, Ni^{2+}, Mn^{2+}, Mg^{2+}, Cd^{2+}, Cu^{2+}, Zn^{2+}, Fe^{3+}, Cr^{3+}, Al^{3+} in their unimer state (10 mM HEPES aqueous solution, pH 7.4) at 25 °C were performed using the fluorescence spectroscopic technique. As shown in Fig. 1, the multifunctional visual thermo-sensor itself no fluorescence emission, but the strong fluorescent emission were observed at 553 nm (λ_{ex}=520 nm) and 448 nm (λ_{ex}=380 nm) upon addition of Fe^{3+} (6 equiv) and Al^{3+} (4 equiv) to the solution of the multifunctional visual thermo-sensor. Furthermore, the addition of Fe^{3+} of the solution shows yellow fluorescence and the addition of Al^{3+} of the solution is blue fluorescence, respectively, which were visible to the naked eye. On the one hand, the primitive BDMa of PEG_{113}-b-P(NIPAM-co-BDMa)$_{60}$ can react with Al^{3+} to produce blue fluorescence. The bonding mode may be that BDMa is chelated with Al^{3+} through interactions with the oxygen atom of C = O, imine nitrogen, and oxygen of phenolic hydroxyl group to forms a rigid system [30, 31]. On the other hand, the spironolactam moiety of the rhodamine group of PEG_{113}-b-P(NIPAM-co-Rh6GEMa)$_{67}$ is used as a signal switch, that is, when Fe^{3+} ions are added, the amide group of the ethylenediamine moiety and the cyclic amide of the spironolactam ring moiety can be coordinated for Fe^{3+} binding, resulting in an appearance of visible yellow fluorescence [32-34]. In contrast, other common metal ions (K^+, Na^+, Li^+, Ca^{2+}, Sr^{2+}, Ba^{2+}, Co^{2+}, Fe^{2+}, Ni^{2+}, Mn^{2+}, Mg^{2+}, Cd^{2+}, Cu^{2+}, Zn^{2+}, Cr^{3+}) did not result in a significant fluorescence change of the multifunctional visual thermo-sensor. The results indicated that the multifunctional visual thermo-sensor can be used for selective detection of Al^{3+} and Fe^{3+} through difference fluorescence response sign.

View Article Online
DOI: 10.1039/C8NJ01917G

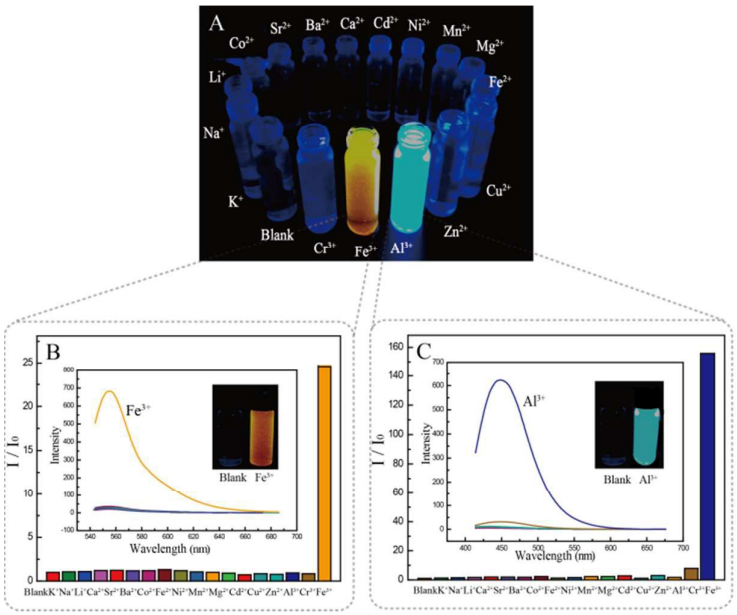

Fig. 1. (A) Optical photographs recorded under UV light (365 nm) after the addition of (K^+, Na^+, Li^+, Ca^{2+}, Sr^{2+}, Ba^{2+}, Co^{2+}, Fe^{2+}, Ni^{2+}, Mn^{2+}, Mg^{2+}, Cd^{2+}, Cu^{2+}, Al^{3+}, Cr^{3+}, Zn^{2+}, Fe^{3+}, 6 equiv of [Rh6GEMa]), respectively for the mixed micelles, (B) Variation of relative fluorescence intensity after the addition of 6 equiv metal ions (λ_{ex}=520 nm), (C) Variation of relative fluorescence intensity after the addition of 4 equiv metal ions. (λ_{ex}=380 nm) (the mixed micelles composed of 0.05 g/L PEG_{113}-b-P(NIPAM-co-BDMa)$_{60}$, [BDMa]=5.02 μM and 0.05 g/L PEG_{113}-b-P(NIPAM-co-Rh6GEMa)$_{67}$, [Rh6GEMa]=14.98 μM; 25 ^oC, pH 7.4; slit widths: Ex. 5 nm, Em. 5 nm)

3.2 Fluorescence titration experiments

In order to verify the sensitivity of the multifunctional visual thermo-sensor, the fluorescence titration experiments were carried out and the results are shown in Fig.2. From the results it can be seen that the corresponding fluorescence intensity gradually increase with the increase of the concentration of target metal ions. The emission intensity of the multifunctional visual thermo-sensor gradually increased with the increase of Fe^{3+} concentration at 553 nm (λ_{ex}=520 nm). When 6 equiv Fe^{3+} ions were added, the fluorescence intensity was saturated and no further increased. Similarly, with the addition of 4 equiv Al^{3+} ions, the fluorescence intensity of the multifunctional visual thermo-sensor at 448 nm (λ_{ex}=380 nm) was observed to increase and reached saturation. In addition, there is a good linear relationship between fluorescence intensity and target metal ion concentration within a certain concentration range. The corresponding lower detection limits were also calculated by

View Article Online
DOI: 10.1039/C8NJ01917G

the formula of (LOD=3σ/slope, σ is the standard deviation of 15 blank samples) to be 30.30 nM (Fe^{3+}) and 5.95 nM (Al^{3+}). Comparing these values with other literature (see Table 3), the results show that the multifunctional visualized temperature-sensitive sensor can detect trivalent metal ions (Fe^{3+} or Al^{3+}) at the nanomolar level.

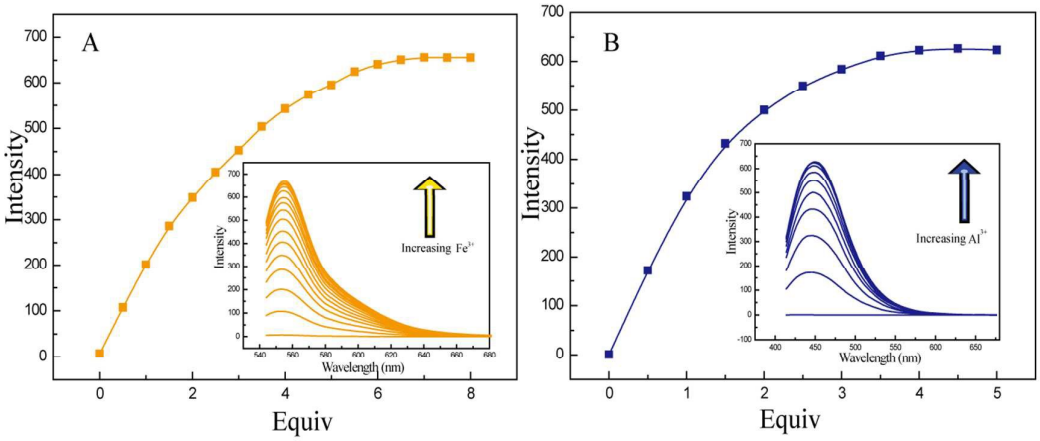

Fig. 2. (A) Changes of the emission intensity with the addition of Fe^{3+} (0-8 equiv of [Rh6GEMa]) at 553 nm (λ_{ex}=520 nm) within 5 h and (B) Changes of the emission intensity with the addition of of Al^{3+} (0-5 equiv of [BDMa]) at 448 nm (λ_{ex}=380 nm). (the mixed micelles composed of 0.05 g/L PEG_{113}-b-P(NIPAM-co-BDMa)$_{60}$, [BDMa]=5.02 μM and 0.05 g/L PEG_{113}-b-P(NIPAM-co-Rh6GEMa)$_{67}$, [Rh6GEMa]=14.98 μM; 25 °C, pH 7.4; slit widths: Ex. 5 nm, Em. 5 nm)

Table 3 Comparison of detection limits and reaction times between current chemical sensors and existing trivalent metal ion chemical sensors

Detected metal ions	Detection Limit	Reaction Time	References
Fe^{3+} , Al^{3+}	4.30, 3.90 umol/L	dependent on carbonate concentration	21
Fe^{3+} , Al^{3+}	45,10 umol/L	\	22
Fe^{3+} , Al^{3+}	2.16, 3.14 umol/L	\	23
Fe^{3+} , Al^{3+}	0.2, 0.3 mmol/L	\	35
Fe^{3+} , Al^{3+}	30, 50 nmol/L	\	36
Fe^{3+} , Al^{3+}	12, 86 nmol/L	20min, 3min	37
Fe^{3+} , Al^{3+}	30.30, 5.95 nmol/L	150s	this work

3.3 Effect of the reaction time

The time-dependent effect of the multifunctional visual thermo-sensor on the Fe^{3+} and Al^{3+} is shown in Fig. 3. When 6 equiv of Fe^{3+} ions were added, the

View Article Online
DOI: 10.1039/C8NJ01917G

fluorescence intensity of the multifunctional visual thermo-sensor increased in the short term and reached the maximum at 150s, and then remained stable. In addition, when 4 equiv of Al^{3+} ions were added, the fluorescence intensity of the multifunctional visual thermo-sensor reached the maximum and remained stable within 80 s. These results indicated that the mixed micelles can effectively and rapidly determine Fe^{3+} and Al^{3+}. In conclusion, the optimal reaction time of the system is 150s (see Table 3).

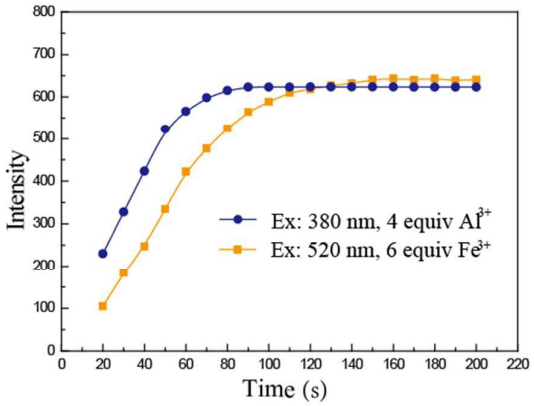

Fig. 3 Time-dependent changes of fluorescence intensity of 4 equiv Al^{3+} and 6 equiv Fe^{3+}, respectively (the mixed micelles composed of 0.05 g/L PEG_{113}-b-P(NIPAM-co-BDMa)$_{60}$, [BDMa]=5.02 μM and 0.05 g/L PEG_{113}-b-P(NIPAM-co-Rh6GEMa)$_{67}$, [Rh6GEMa]=14.98 μM; 25°C, pH 7.4; slit widths: Ex. 5 nm, Em. 5 nm).

3.4 Effect of the system temperature

It is well known that the low critical solution temperature (LCST) of the thermally stable triblock copolymer can be easily adjusted to the desired value by incorporating hydrophobicity or hydrophobic repeating units into a thermoresponsive block such as Poly N-Isopropylacrylamide (PNIPAM)[38]. In the current work, thermo-induced self-assembling and disassembly behavior of the multifunctional visual thermo-sensor was investigated. Temperature-dependent optical transmittance was employed at first to determine the LCST (Fig. 4 A). It could be found that the phase transition behavior occurs when the temperature was higher than the LCST of 36.0 °C from the test. In addition, the result of dynamic laser light scattering (DLS) (as shown in Fig. 4 B) also confirmed this point. The result of DLS showed that when the temperature was 40.0 °C, the multifunctional visual thermo-sensor in aqueous

View Article Online
DOI: 10.1039/C8NJ01917G

solution could self-assemble into aggregates with P (NIPAM-co-BDMa) and P (NIPAM-co-R6GEMa) as the nucleus. Its <Dh> was 166.5 nm, and the polydispersity index of the particle size was 0.24.

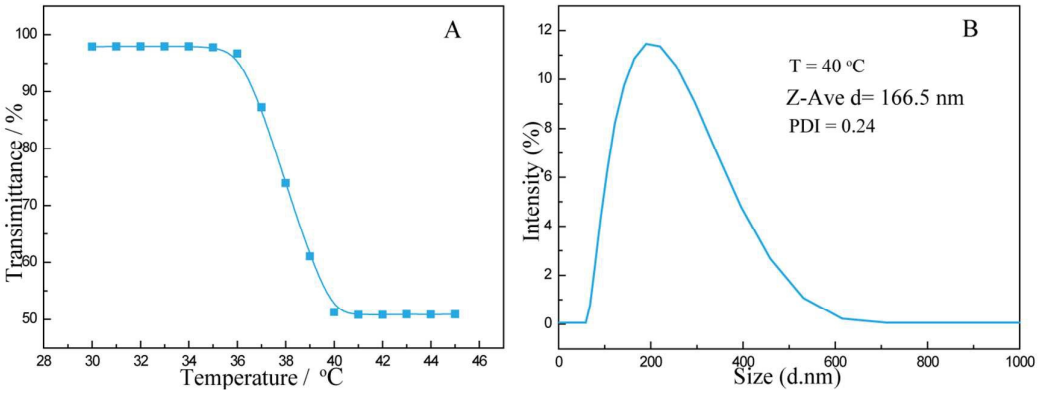

Fig. 4 (A) Temperature-dependence of optical transmittance recorded at a wave of 700 nm and (B) Intensity average hydrodynamic diameter distributions of mixed micelles composed of 0.05g/L PEG_{113}-b-P(NIPAM-co-BDMa)$_{60}$ and 0.05g/L PEG_{113}-b-P(NIPAM-co-Rh6GEMa)$_{67}$.

Based on the characteristics of temperature sensitivity, theoretically the multifunctional visual thermo-sensor could self-assemble under the induction of temperature to form mixed micelles in aqueous solution. The metal ion detection element will be located within the hydrophobic nucleus, whereas the organic dye will generally have a stronger fluorescence in a hydrophobic environment than in a hydrophilic environment [39-41]. This will increase the quantum yield of the fluorescent elements to achieve signal amplification. As shown in Fig. 5, the fluorescence intensity at 552 nm (λ_{ex}=520 nm) in the presence of 6 equiv Fe^{3+} was significantly enhanced with the increase of temperature (20-45 °C); while the fluorescence intensity at 448 nm (λ_{ex}=380 nm) was also significantly enhanced with the increase of temperature (20-45 °C) in the presence of 4 equiv Al^{3+} as shown in Fig. 6. The fluorescence intensity of Fe^{3+} and Al^{3+} was amplified by 2.43 and 2.59 times respectively at 40 °C compared with 25 °C. In particular, the detection limit of the multifunctional visual thermo-sensor for Fe^{3+} increased from 30.30 to 23.84 nM, and the detection limit of Al^{3+} increased from 5.95 to 4.02 nM as the temperature increased. It is worth mentioning that the fluorescence enhancement could be observed only when the temperature is higher than the LCST (36 °C) of the mixed

View Article Online
DOI: 10.1039/C8NJ01917G

micelles, which is consistent with the critical micelle temperature obtained by the experiment of light transmittance and temperature dependence. In summary, the temperature-induced copolymer self-assembly can significantly improve the sensitivity of the detection by embedding the metal ion detection element into the thermosensitive block.

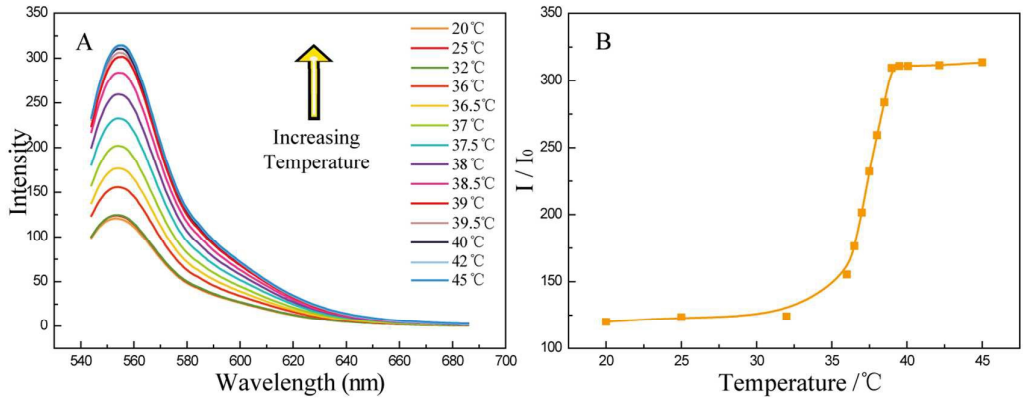

Fig. 5 (A) and (B) Temperature-dependence fluorenscence spectra and change in fluorenscence intensity at a wave of 552 nm (λ_{ex}=520 nm) after the addition of 6 equiv Fe^{3+} (the mixed micelles composed of 0.05 g/L PEG_{113}-b-P(NIPAM-co-BDMa)$_{60}$, [BDMa]=5.02 μM and 0.05 g/L PEG_{113}-b-P(NIPAM-co-Rh6GEMa)$_{67}$, [Rh6GEMa]=14.98 μM; pH 7.4; λ_{ex}=520 nm, slit widths: Ex. 5 nm, Em. 2.5 nm)

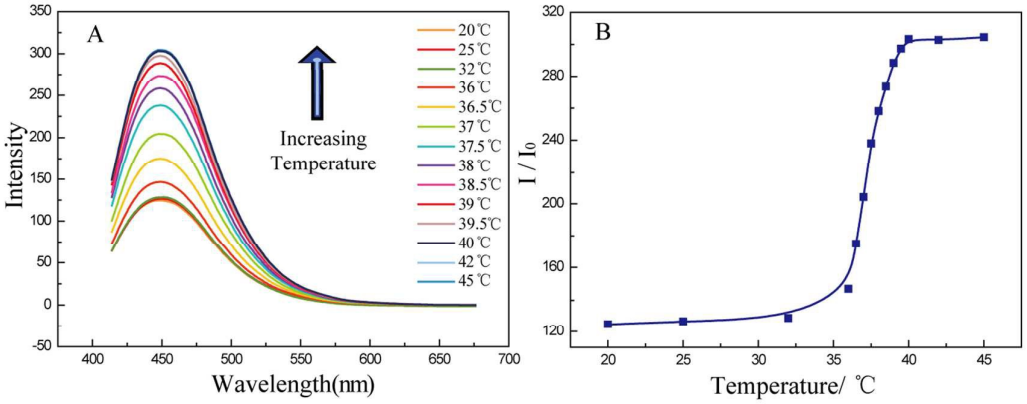

Fig. 6 (A) and (B) Temperature-dependence fluorenscence spectra and change in fluorenscence intensity at a wave of 448 nm (λ_{ex}=380 nm) after the addition of 4 equiv Al^{3+} (the mixed micelles composed of 0.05 g/L PEG_{113}-b-P(NIPAM-co-BDMa)$_{60}$, [BDMa]=5.02 μM and 0.05 g/L PEG_{113}-b-P(NIPAM-co-Rh6GEMa)$_{67}$, [Rh6GEMa]=14.98 μM; pH 7.4; λ_{ex}=380 nm, slit widths: Ex. 5 nm, Em. 2.5 nm)

3.5 Fluorescence competitive experiments

View Article Online
DOI: 10.1039/C8NJ01917G

In order to verify the unique selectivity and high sensitivity of the multifunctional visual thermo-sensor toward Fe^{3+} and Al^{3+} ions, the interference experiments with other common metal ions were carried out and the results are shown in Fig. 7. As shown in Fig. 7 A, the addition of interfering ions hardly changes the fluorescence intensity of sensor-Fe^{3+} complex at 553 nm (λ_{ex}=520 nm). But in Fig. 7B, the addition of other interfering ions (K^+, Na^+, Li^+, Ca^{2+}, Sr^{2+}, Ba^{2+}, Co^{2+}, Fe^{2+}, Ni^{2+}, Mn^{2+}, Mg^{2+}, Cd^{2+}, Cu^{2+}, Zn^{2+}, Fe^{3+}, Cr^{3+}) almost did not change the fluorescence intensity of sensor-Al^{3+} complex at 448 nm (λ_{ex}=380 nm) except for Fe^{2+}, Cu^{2+} and Fe^{3+}. Fe^{2+}, Cu^{2+} and Fe^{3+} can quench part of the fluorescence (about 73%, 93% and 53%, respectively) in the mixed micellar solution. These features allow the mixed micelles to qualitatively and quantitatively analyze the coexistence of Al^{3+} and Fe^{3+} ions. In addition, further accurate quantification of Al^{3+} in the presence of Fe^{2+}, Cu^{2+} and Fe^{3+} ions shall rely on the removal of Fe^{2+}, Cu^{2+} and Fe^{3+} at first by the use of strong chelating ligands such as EDTA (ethyl-diacetic acid tetraacetic acid) -activated resin to remove interfering ions.

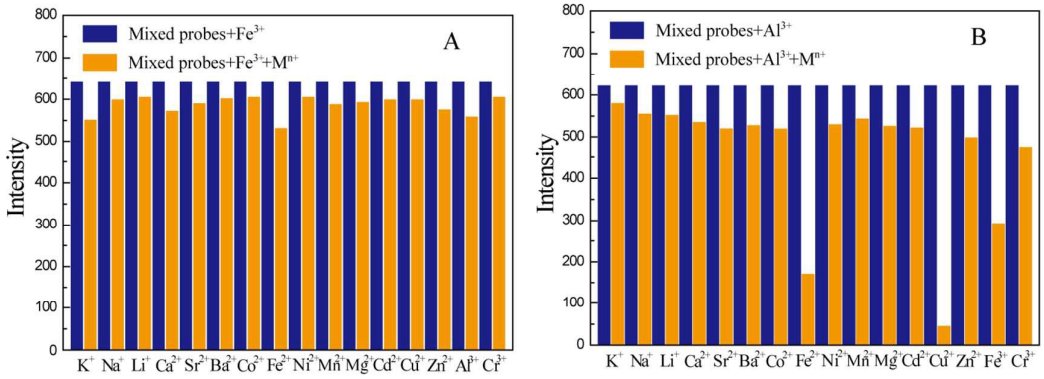

Fig. 7 Effect of equal concentration of competitive metal ions on the interaction between mixed micelles and (A) Fe^{3+} ion (15 μmol/L) and (B) Al^{3+} ion (5 μmol/L) (the mixture micelles composed of 0.05 g/L PEG_{113}-b-P(NIPAM-co-BDMa)$_{60}$, [BDMa]=5.02 μM and 0.05 g/L PEG_{113}-b-P(NIPAM-co-Rh6GEMa)$_{67}$, [Rh6GEMa]=14.98 μM; 25 ^{o}C, pH 7.4; (A) λ_{ex}=520 nm, (B)=380 nm, slit widths: Ex. 5 nm, Em. 5 nm).

3.6 Moulds for qualitative and quantitative detection of metal ion mixtures

Since the multifunctional visual thermos-sensor can selectively identify Al^{3+} (blue fluorescence) and Fe^{3+} (yellow fluorescence), a visual detection method was

View Article Online
DOI: 10.1039/C8NJ01917G

constructed by mixing a certain amount of Al^{3+} and Fe^{3+} to produce different fluorescent colors. Specially, based on the original diagram (Fig. 8A) obtained by mixing the metal ions and the characteristic diagram (Fig. 8B) relied on the difference of fluorescence RGB before and after the reaction, the predictive models were established through PCA and regression analysis, which can realize the simultaneous quantitative detection of mixed ions with Al^{3+} and Fe^{3+} in aqueous solution. In addition, the qualitative mechanism could be expanded with the refinement of the mixed ion ratio.

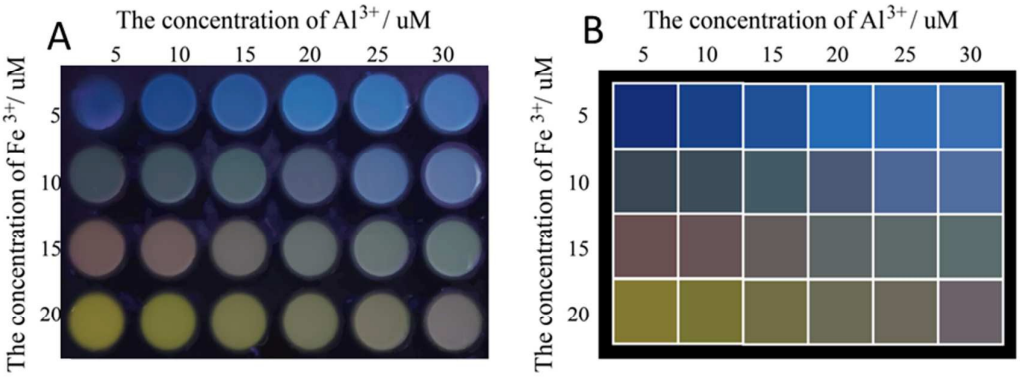

Fig. 8. Picture of original diagram (A) and RGB color difference (B) of different mixing ratio of Fe^{3+} and Al^{3+} under UV.

In this paper, SPSS (Statistical Product and Service Solutions) 20 software was used for PCA, the value of the factor of the four models saved as variables (see Table S1). In the table, only the first principal component of the models is greater than 1 (2.885, 2.938, 2.970, 2.897, respectively). The variance contribution rate is 96.175%, 97.936%, 99.202% and 96.551% respectively (When the cumulative contribution rate of the principal component reaches 85%, the valid information can be retained), which indicates that the first principal component contains all the information of three indexes, and is most mainly affected by the ratio of Al^{3+} and Fe^{3+}. From the scree plot (see Fig. S3), it can be seen that the second eigenvalue of the four models is about zero, that is, the trend of change has begun to flatten. Thus, only one principal component is appropriate for the four models, and then the load is calculated for the first principal component (see Table S2).

Finally, the multiple linear regression analysis and the reduction of variables are

View Article Online
DOI: 10.1039/C8NJ01917G

used to obtain the models of Quantitative Structure-Pharmacokinetics Relationship (QSPR) as shown in Table 4. The degree of influence of the three independent variables on the dependent variable is compared according to the coefficients in Table 4. The sign of the coefficient indicates the direction of influence, and the larger the absolute value of the coefficient, the greater the effect.

Table 4 Parametric equations of model 1-4

Rows	QSPR Moulds
1	I=0.0478ΔR+0.0209ΔG+0.0151ΔB−2.9077
2	I=0.0302ΔR+0.0183ΔG+0.0089ΔB−3.1937
3	I=-0.0456ΔR+0.0263ΔG+0.0289ΔB+0.9891
4	I=-0.0157ΔR−0.0203ΔG+0.0071ΔB+4.3843

3.7 Verification test of predictive models

The relationships between the predicted scales and the actual value content calculated from the models are listed in Fig. 9. The actual values represented the exact contents of Al^{3+} and Fe^{3+} mixed ions, and the predicted values were the predicted contents of Al^{3+} and Fe^{3+} mixed ions calculated from the principal component regression models. The results showed that the slopes of all images were close to 1, and four quantitative models had high R^2 values (0.9966-0.9998). This indicated that the principal component regression models constructed by the experimental color difference data had a good accuracy for predicting the contents of Al^{3+} and Fe^{3+} mixed ions. RMSE (Root Mean Square Error) is a good way to reflect the accuracy of the measurement, the smaller the RMSE values, the higher the accuracy of measurement. The RMSE values of the four principal component regression quantitative models in Fig. 9 are between 0.0167 and 0.0714, the RMSE values obtained are lower, indicating that the models established in this experiment are more accurate. Therefore, the four principal component regression quantitative models established in this experiment can be used to predict the ion contents of Al^{3+} and Fe^{3+} mixed ions accurately.

View Article Online
DOI: 10.1039/C8NJ01917G

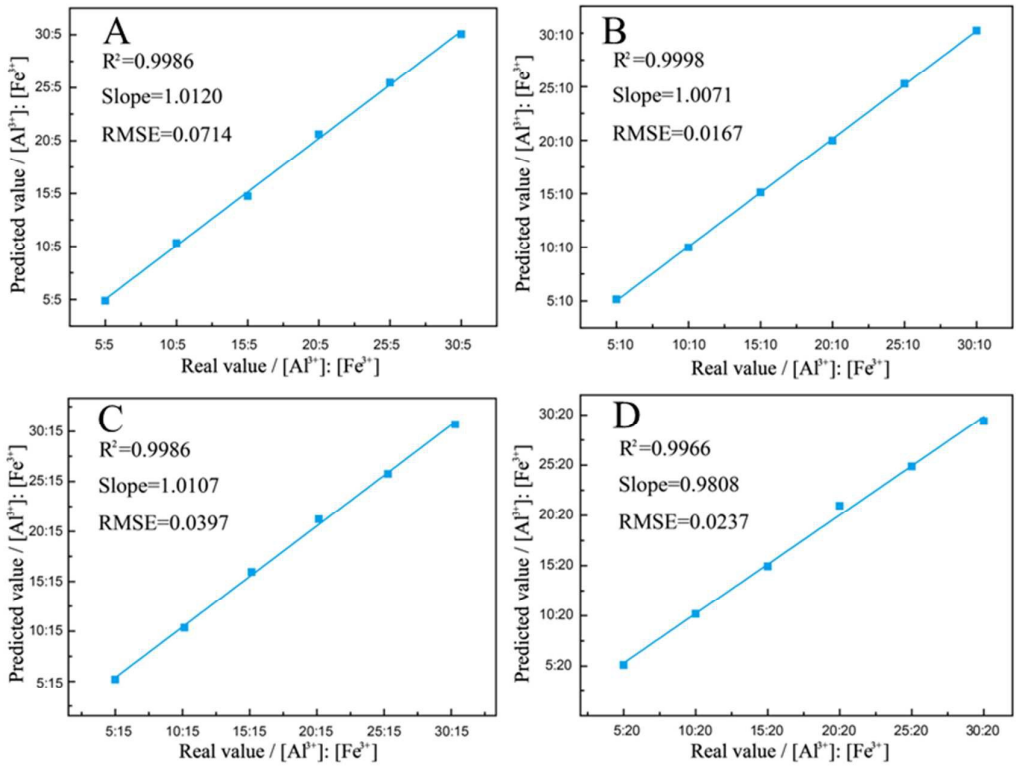

Fig. 9. The relationship between the predicted mixed metal ion ratio and the actual ratio for these four models, (A) Model 1, (B) Model 2, (C) Model 3, (D) Model 4

4. Conclusion

This paper prepared a novel multifunctional visual thermo-sensor based on two amphiphilic block polymers , that were PEG_{113}-b-P(NIPAM-co-BDMa)$_{60}$, PEG_{113}-b-P(NIPAM-co-Rh6GEMa)$_{67}$, which were labeled with Al^{3+} and Fe^{3+} recognition elements BDMa and Rh6GEMa in thermosensitive block, respectively. The synthetic mixed micelles can be used as a multifunctional visual thermo-sensor to Al^{3+}, Fe^{3+} and temperature. The detection sensitivity to Al^{3+} and Fe^{3+} ions can be considerably enhanced at elevated temperatures via the formation of hydrophobic domains within thermo-induced micellar aggregates of DHBCs. As the temperature increased from 25.0 ^{o}C to 40.0 ^{o}C, the detection limit of 0.05 g/L mixed micelles for the analysis of Al^{3+} ions reduced from ~5.95 nM to ~4.02 nM, and Fe^{3+} ions reduced from ~30.30 nM to ~23.84 nM, respectively. Furthermore, the mixed micelles were successfully coupled with PCA analysis method to build predictive models to achieve rapid quantitative detection of mixed metal ions with Al^{3+} and Fe^{3+}. In addition, the

View Article Online
DOI: 10.1039/C8NJ01917G

predictive models were verified by given concentration of Al^{3+} and Fe^{3+} and the accuracy is very high. The multifunctional visual thermo-sensor in the current study can offer a series of potential features such as improved water solubility, enhanced detection sensitivity, excellent biocompatibility and quantitative simultaneous detection of Al^{3+} and Fe^{3+}.

Fundings

This work was supported by the National Natural Science Foundation of China (Nos. 31470434, 21576124, 21507047 and 21676124), China Postdoctoral Science Foundation (No. 2017M610308), Postdoctoral Science Foundation of Jiangsu Province (No. 1701107B), the Science Foundation of State General Administration of the People's Republic of China for Quality Supervision and Inspection and Quarantine (No.2017IK139) and Zhenjiang Social development project (No. SH2016019).

References

1. K. Vijay, C. Nandi and S. Samant, *Rsc Advances*, 2016, **6**, 49724-49729.
2. L. Wang, H. Li and D. Cao, *Sensors & Actuators B:chemical*, 2013, **181**, 749-755.
3. R. Wang, Q. Wan, F. Feng and Y. Bai, *Chemical Research in Chinese Universities*, 2014, **30**, 560-565.
4. M. M. Zhu, C. X. Shi, X. T. Xu, Z. Guo and W. Zhu, *Rsc Advances*, 2016, **6**, 1-7.
5. J. L. Bricks, A. Kovalchuk, C. Trieflinger, M. Nofz, M. Büschel, A. I. Tolmachev, J. Daub and K. Rurack, *Journal of the American Chemical Society*, 2005, **127**, 13522-13529.
6. Z. Chen, Y. Sun, L. Zhang, D. Sun, F. Liu, Q. Meng, R. Wang and D. Sun, *Chemical Communications*, 2013, **49**, 11557-11559.
7. S. Goswami, A. Manna, S. Paul, K. Aich, A. K. Das and S. Chakraborty, *Dalton Transactions*, 2013, **42**, 8078-8085.
8. H. Kozlowski, A. Janicka-Klos, J. Brasun, E. Gaggelli, D. Valensin and G.

View Article Online
DOI: 10.1039/C8NJ01917G

Valensin, *Coordination Chemistry Reviews*, 2009, **253**, 2665-2685.

9. S. Dang, E. Ma, Z. M. Sun and H. Zhang, *Journal of Materials Chemistry*, 2012, **22**, 16920-16926.

10. J. W. Lee and J. D. Helmann, *Nature*, 2006, **440**, 363-367.

11. F. Bousejraelgarah, C. Bijani, Y. Coppel, P. Faller and C. Hureau, *Inorganic Chemistry*, 2011, **50**, 9024-9030.

12. Elizabeth M. Nolan, Jubin W. Ryu, Jacek Jaworski, Rodney P. Feazell, Morgan Sheng and Stephen J. Lippard, *Journal of the American Chemical Society*, 2006, **128**, 15517-15528.

13. L. He, V. L. L. So and J. H. Xin, *Sensors & Actuators B Chemical*, 2014, **192**, 496-502.

14. C. R. Lohani, J. M. Kim, S. Y. Chung, J. Yoon and K. H. Lee, *Analyst*, 2010, **135**, 2079-2084.

15. X. Chen, X. Y. Shen, E. Guan, Y. Liu, A. Qin, J. Z. Sun and B. Z. Tang, *Chemical Communications*, 2013, **49**, 1503-1505.

16. K. B. Kim, D. M. You, J. H. Jeon, Y. H. Yeon, J. H. Kim and C. Kim, *Tetrahedron Letters*, 2014, **55**, 1347-1352.

17. Z. Li, Q. Hu, C. Li, J. Dou, J. Cao, W. Chen and Q. Zhu, *Tetrahedron Letters*, 2014, **55**, 1258-1262.

18. J. Mao, L. Wang, W. Dou, X. Tang, Y. Yan and W. Liu, *Organic Letters*, 2007, **9**, 4567-4570.

19. X. Tang, Y. Wang, J. Han, L. Ni, L. Wang, L. Li, H. Zhang, C. Li, J. Li and H. Li, *Spectrochim Acta A Mol Biomol Spectrosc*, 2017, **191**, 172-179.

20. L. Wang, W. Li, W. Zhi, Y. Huang, J. Han, Y. Wang, Y. Ren and L. Ni, *Sensors & Actuators B Chemical*, 2018, **260**, 243-254.

21. L. He, C. Liu and J. H. Xin, *Sensors & Actuators B Chemical*, 2015, **213**, 181-187.

22. Y. Kang, X. J. Zheng and L. P. Jin, *J Colloid Interface Sci*, 2016, **471**, 1-6.

23. S. Suganya, W. N. Jin, A. K. Mutyala, S. Velmathi, J. P. Kim and J. S. Park,

View Article Online
DOI: 10.1039/C8NJ01917G

Journal of Photochemistry & Photobiology A Chemistry, 2017, **344**, 36-41.

24. J. Hu, L. Dai and S. Liu, *Macromolecules*, 2011, **44**, 4699-4710.

25. J. Hu, T. Wu, G. Zhang and S. Liu, *Macromolecules*, 2012, **45**, 3939-3947.

26. K. Li, Y. Xiang, X. Wang, J. Li, R. Hu, A. Tong and B. Z. Tang, *Journal of the American Chemical Society*, 2014, **136**, 1643-1649.

27. S. Samanta, U. Manna, T. Ray and G. Das, *Dalton Transactions*, 2015, **44**, 18902-18910.

28. Y. Song, W. Zhang, Y. An, L. Cui, C. Yu, Z. Zhu and C. J. Yang, *Chemical Communications*, 2012, **48**, 576-578.

29. Y. Wang, Y. Li, X. Bao, J. Han, J. Xia, X. Tian and L. Ni, *Talanta*, 2016, **160**, 194-204.

30. A. A. A. Aziz, R. G. Mohamed, F. M. Elantabli and S. M. Elmedani, *Journal of Fluorescence*, 2016, **26**, 1927-1938.

31. Q. Zhang, H. Wang, Y. Wang, P. Jing, A. Luo and Q. Huang, *Research on Chemical Intermediates*, 2016, **42**, 1-13.

32. X. Chen, T. Pradhan, F. Wang, J. S. Kim and J. Yoon, *Chemical Reviews*, 2012, **112**, 1910-1956.

33. H. Kim, B. A. Rao, J. Jeong, S. Angupillai, J. S. Choi, J. O. Nam, C. S. Lee and Y. A. Son, *Sensors & Actuators B Chemical*, 2016, **224**, 404-412.

34. Q. Meng, W. Su, X. Hang, X. Li, C. He and C. Duan, *Talanta*, 2011, **86**, 408-414.

35. X. Mu, L. Qi, J. Qiao and H. Ma, *Analytical Methods*, 2014, **6**, 6445-6451.

36. N. R. Chereddy, P. Nagaraju, M. V. Niladri Raju, V. R. Krishnaswamy, P. S. Korrapati, P. R. Bangal and V. J. Rao, *Biosensors & Bioelectronics*, 2015, **68**, 749-756.

37. X. Fang, S. Zhang, G. Zhao, W. Zhang, J. Xu, A. Ren, C. Wu and W. Yang, *Dyes & Pigments*, 2014, **101**, 58-66.

38. O. Soga, C. F. V. Nostrum, A. Ramzi, T. Visser, F. Soulimani, P. M. Frederik, P. H. H. Bomans and W. E. Hennink, *Langmuir: the Acs Journal of Surfaces &*

View Article Online
DOI: 10.1039/C8NJ01917G

Colloids, 2004, **20**, 9388-9395.

39. K. Iwai, Y. Matsumura, S. Uchiyama and A. P. D. Silva, *Journal of Materials Chemistry*, 2005, **15**, 2796-2800.

40. Y. Shiraishi, R. Miyamoto, X. Zhang and T. Hirai, *Organic Letters*, 2007, **9**, 3921-3924.

41. Y. Shiraishi, A. Ryo Miyamoto and T. Hirai, *Langmuir: the Acs Journal of Surfaces & Colloids*, 2008, **24**, 4273-4279.